Quaternary Research 74 (2010) 132–144

Contents lists available at ScienceDirect

Quaternary Research

journal homepage: www.elsevier.com/locate/yqres

Quaternary glaciation in the Nubra and Shyok valley confluence, northernmost Ladakh, India

Jason M. Dortch [a,*], Lewis A. Owen [a], Marc W. Caffee [b]

[a] Department of Geology, University of Cincinnati, Cincinnati, OH45221, USA
[b] Dept of Physics/PRIME Laboratory, Purdue University, West Lafayette, IN 47906, USA

ARTICLE INFO

Article history:
Received 13 November 2009

Keywords:
Himalaya
Karakoram
Ladakh Range
Mountain glaciation
Geochronology
Moraines
Cosmogenics
ELA

ABSTRACT

Three glacial stages (Deshkit 1, Deshkit 2 and Dishkit 3 glacial stages) are identified in the Nubra and Shyok valleys in northernmost Ladakh, northwest India, on the basis of geomorphic field mapping, remote sensing, and ^{10}Be terrestrial cosmogenic nuclide surface exposure dating. The glacial stages date to ~45 ka (Deshkit 1 glacial stage), ~81 ka (Deshkit 2 glacial stage) and ~144 ka (Deshkit 3 glacial stage). A mean equilibrium line altitude depression of ~290 m for the Deshkit 1 glacial stage was calculated using the area accumulation ratio, toe-to-headwall ratio, area–altitude, and area–altitude balance ratio methods. Comparison of glaciation in the Nubra and Shyok valleys with glaciations in the adjacent Central Karakoram of northern Pakistan and northern side of the Ladakh Range of northern India indicates that glaciation was synchronous on Milankovitch timescales across the region during MIS-6, but differed greatly in extent, with more extensive glaciation in the Karakoram than the morphostratigraphically equivalent glaciation on the northern slopes of the Ladakh Range. This highlights the strong contrast in the extent of glaciation across ranges in the Himalaya–Tibetan orogen, necessitating caution when correlating glacial successions within and between mountain ranges.

© 2010 Univesity of Washington. Published by Elsevier Inc. All rights reserved.

Introduction

During the last decade, numerical dating methods utilizing terrestrial cosmogenic nuclide surface exposure and luminescence dating have illustrated the complexity of glacial successions and glaciation in the Himalayan–Tibetan orogen (e.g. Owen et al., 2001, 2003, 2008, 2009; Phillips et al., 2000; Richards et al., 2000a, b; Seong et al., 2007, 2009; Zech et al., 2000, 2003, 2005). These studies indicate that contrasting patterns of glaciation exist across adjacent regions of the Himalaya, which are likely due to a combination of orographic and climatic influences (Owen et al., 2008). Accordingly, the investigation of these variations in the patterns of glaciation requires the development of regional-scale glacial chronologies. As part of this endeavor, we examine glacial geologic records in the Nubra and Shyok valleys in northernmost Ladakh of northwest India using geomorphic mapping, aided by remote sensing, and ^{10}Be terrestrial cosmogenic nuclide surface exposure dating of glacial landforms (Fig. 1). Northernmost Ladakh is an ideal study area because: 1) the adjacent regions have been the focus of prior glacial geologic studies that can be used to examine regional differences in glaciation; 2) the semi-arid climate of the region preserves a long and detailed glacial record; and 3) the region is relatively accessible.

Regional setting

The Nubra and Shyok valleys are situated in the Transhimalaya and span the Central Karakoram and Ladakh Range of northwest India and northern Pakistan (Fig. 1). The region is bisected by the Karakoram Fault, a NW trending, continental scale, right-lateral strike-slip fault separating the Central Karakoram and Ladakh Range (Dunlap et al., 1998; Searle et al. 1998, Searle and Richard, 2007; Chevalier et al., 2005). The Central Karakoram contains four >8000 m peaks (K2 at 8611 m above sea level [a.s.l.], Gasherbrum 1 at 8068 m a.s.l., Gasherbrum 2 at 8034 m a.s.l., and Broad Peak at 8047 m a.s.l.) and is heavily glaciated. Two major glacial systems, the Baltoro and Siachen, extend for ~55 km and ~70 km throughout the Central Karakoram, respectively, and >30 glaciers longer than 20 km are found within the range. The valleys of the Central Karakoram are deeply incised, with a relative relief of ≥5000 m. In contrast, the Ladakh Range has a relative relief of 1000 m to 2000 m, with few peaks higher than 7000 m a.s.l. Glaciers in the Ladakh Range are generally restricted to cirques and are typically <4.5 km long.

Precipitation in the Central Karakoram is dominated by the mid-latitude westerlies, with 2/3 of the precipitation occurring during winter (Hewitt, 1989). The peaks of the NW Lesser Himalaya, with a

* Corresponding author.
E-mail address: Dortchjm@mail.uc.edu (J.M. Dortch).

0033-5894/$ – see front matter © 2010 Univesity of Washington. Published by Elsevier Inc. All rights reserved.
doi:10.1016/j.yqres.2010.04.013

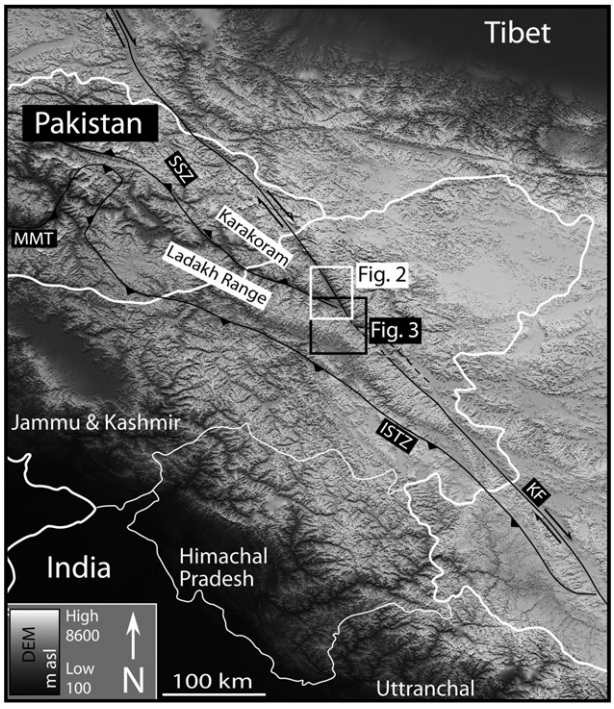

Fig. 1. Hillshade SRTM DEM with location of study area in northern India and northern Pakistan.

mean topographic profile of >4000 m a.s.l., significantly reduce monsoon-driven moisture transport to the Central Karakoram and Ladakh Range (Bookhagen et al., 2005; Bookhagen and Burbank 2006). Nonetheless, the Ladakh Range receives most of its precipitation from the south Asian summer monsoon (Gasse et al., 1996; Brown et al., 2003; Owen et al., 2006). Precipitation likely increased in the Karakoram and Ladakh Ranges during past episodes of enhanced monsoons (Gasse et al., 1996; Shi et al., 2001).

Seong et al. (2007) defined four glacial stages in the Central Karakoram along the Baltoro, Panmah, Chogo Lungma, and Biafo glacial systems, and suggested that regional glacial fluctuations are controlled by the mid-latitude westerlies and oscillation in the Northern Hemisphere ice sheets and oceans. Owen et al. (2006) defined five glacial stages in the Ladakh Range, and in contrast, suggested that glaciation was primarily controlled by the south Asian summer monsoon during the past 100 ka. Siachen glacial system is the largest in northwest India. Sourced at the head of the Nubra Valley, on Sia Kangri at 7422 m a.s.l., Siachen glacial system forms a vital link between westerly and monsoon dominated regions at the western end of the Himalayan–Tibetan orogen. However, the timing and extent of glaciation have not previously been defined for this glacial system.

Our work focuses mainly on past-glaciation of the Nubra–Shyok valley confluence on the northern side of the Ladakh Range (Figs. 2 and 3), building on the work of Owen et al. (2006) and Seong et al. (2007). The Nubra Valley is a structurally controlled, SW trending valley, approximately following the main trace of the Karakoram Fault. This valley contains many glacially derived landforms and sediments (Pant et al., 2005; Phartiyal et al., 2005). These include moraines, roche moutonnées, glacial benches, lacustrine sediments, till deposits, alluvial fans, shorelines and dune fields (Fig. 4). The contemporary Siachen Glacier has a thick supraglacial debris cover, typical of large glaciers in the Himalaya and Karakoram (Benn and Owen, 2002). Thick supraglacial debris cover insulates glaciers, reducing the effects of temperature changes, thus making them more responsive to precipitation (Derbyshire, 1981; Shi et al., 2001; Owen and Benn 2005). During the peak ablation season, Siachen Glacier discharges 23×10^6 m^3 d^{-1} of meltwater with a suspended sediment load of 2–3 kg m^{-3} s^{-1} (Bhutiyani, 2000).

Methods

Field methods

Glacial and non-glacial sediments and landforms were identified and mapped in the field using topographic maps generated from 15 m resolution Advanced Spaceborne Thermal Emission and Reflection Radiometer (ASTER) and 3 arc-second (~90 m) Shuttle Radar Topography Mission (SRTM) digital elevation models (DEMs) (CGIAR-CSI, 2007; NASA, 2007). Individual glacier catchments were delineated using ArcGIS 1.1 Hydro software. The extent of the modern glaciers was determined using NASA Worldwind false-color imagery. These images were mapped onto a SRTM DEM in ArcGIS 9.1. The DEM coverage of the contemporary glaciers was isolated, and the surface area was calculated using ArcGIS 9.1 3D Analyst. The raster was imported into ReadArcGrid to calculate the hypsometric integral and to bin elevation areas at 100 m intervals (Nash, 2007). Three relative glacial stages were defined by mapping landforms, defined here as the Deshkit 1 (youngest), Deshkit 2, and Deshkit 3 (oldest) glacial stages (Fig. 4).

Cosmogenic ^{10}Be from quartz rich boulders and bedrock was used to date the glacial landforms. Samples were collected from sites that showed minimal evidence of erosion, especially dissection or deflation. Sites showing patterned ground were not sampled. Two to twelve samples were collected from each landform. About 350 g of rock were collected from the upper surfaces of boulders and bedrock; the sampling depth was from 1 to 5 cm. The location, geomorphic setting, lithology, size, shape, and weathering characteristics of each sampled surface were recorded. Topographic shielding was determined by measuring the inclination from the sampled surface to the surrounding horizon.

^{10}Be surface exposure dating

Standard methods were used for isolation of quartz, chemical separation of Be, and preparation of BeO (c.f. Kohl and Nishiizumi, 1992; Dortch et al., 2008, and references therein). All ^{10}Be ages were calculated using the PRIME Laboratory Rock Age Calculator (Ma et al., 2007; PRIME Laboratory, 2007; Table 1), which employs the scaling factors of Stone (2000) and a sea-level low-latitude production rate of 4.5 ± 0.3 ^{10}Be atoms/gram of quartz/year and a ^{10}Be half life of 1.36 Ma (Nishiizumi et al., 2007). Please see PRIME (2010) for details of converting ^{10}Be ratios to ICN standards of Nishiizumi et al. (2007). No corrections were made for geomagnetic field variations; there is as of yet no agreed upon method for making this correction (Balco et al., 2008a,b; Owen et al., 2008). Geomagnetic corrections can change the ^{10}Be ages reported here by a maximum of 16% using the scaling scheme of Nishiizumi et al. (1989).

The ages presented in Table 1 are modeled exposure ages, assuming no erosion. Erosion rates and exposure ages cannot be determined simultaneously; however, we can estimate the effect of erosion for a range of ages. A limiting erosion rate of 3.7 ± 0.2 m Ma^{-1} is calculated using the boulder with the oldest apparent model age (NU-16). If we assume all sampled boulders erode at that rate, then a calculated age of 10 ka would underestimate the true age by a maximum of 4%, an age of 40 ka by 14%, and an age of 80 ka by 31%. Geomagnetic corrections are systematic and would not significantly affect correlations between landforms in adjacent areas. Erosion rates of boulders are likely similar between the regions; for example, the oldest boulder of Seong et al. (2007) (K2-4 at 168 ± 12 ka recalculated using our methods) for the central Karakoram gives a maximum erosion rate of 3.5 ± 0.1 m Ma^{-1}, which is similar to our rate. To facilitate comparison to adjacent regions,

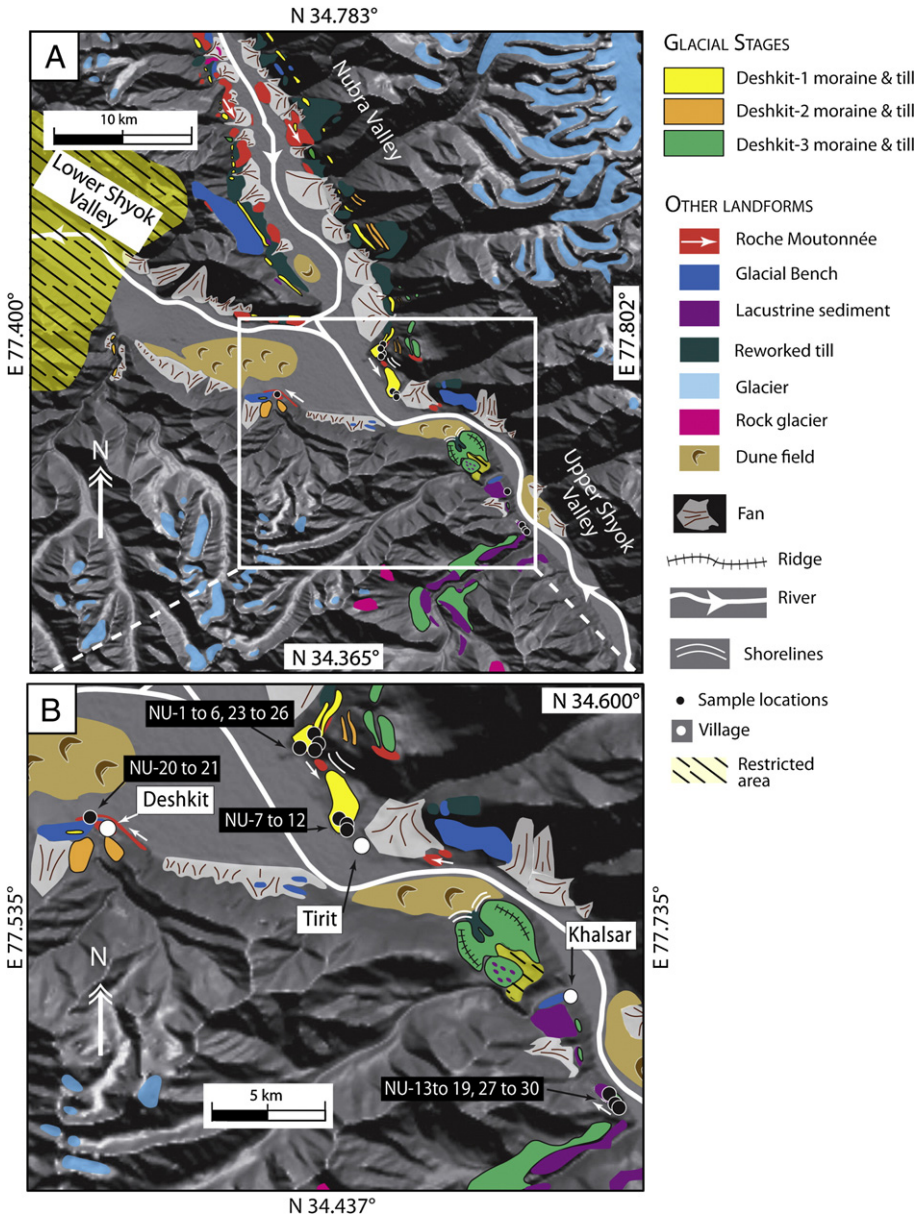

Fig. 2. Hillshade SRTM DEM showing the geomorphology of the Nubra–Shyok confluence. A) Glacial and non-glacial landforms, contemporary glaciers, and location of sampling area. B) Sampling locations and major villages at the confluence of the Nubra and Shyok valleys. The white arrows show the direction of ice movement based on erosional features on the roche moutonnées.

the ^{10}Be ages from Seong et al. (2008) for the Central Karakoram were recalculated with the PRIME Laboratory Rock Age calculator (Table 1).

ELA reconstruction

The difference between contemporary and former ELAs can help quantify glaciation and climate change. The ELA of a glacier is the elevation where seasonal accumulation is equal to ablation; that is, the net mass balance equals zero, over several years or more. Several methods are commonly used to reconstruct ELAs, including area accumulation ratio (AAR), toe-to-headwall accumulation ratio (THAR), area–altitude (AA), area–altitude balance ratio (AABR), and maximum elevation of lateral moraines (MELM) (Benn et al., 2005; Osmaston, 2005). There are numerous issues regarding the use and application of each ELA reconstruction method (Benn and Lehmkuhl, 2000; Benn et al., 2005). These problems have been summarized in detail for glaciers in high altitude mountainous regions, specifically for the Himalaya, by Benn et al. (2005) and Owen and Benn (2005). Benn et al. (2005) suggest that several methods should be used to reconstruct ELAs, and we adopt this approach in our study.

The accumulation/ablation ratios of the AAR, THAR, AA, and AABR methods can vary within and across regions. Catchment area and shape, debris cover, and glacier aspect can all cause variation of reconstructed ELAs. Modern debris-covered glaciers in the Himalaya typically have an AAR of 0.2–0.4 (Müller, 1980; Kulkarni, 1992). In middle and northern latitudes, a THAR of 0.5 is typically used (Benn et al., 2005). Seong et al. (2008) showed that a THAR of 0.5 and an AAR of 0.44 are reliable in the Central Karakoram. This is at the high end of the range used by Müller (1980) and Kulkarni (1992) for other regions of the Himalayan–Tibetan orogen. Furthermore, the AABR method of Osmaston (2005) with a ratio ~1.0 or less can be used for debris-covered glaciers. The AA method works best for glaciers with a simple geometry and few tributaries, but typically yields more reliable results than the AAR and THAR methods (Osmaston, 2005). The

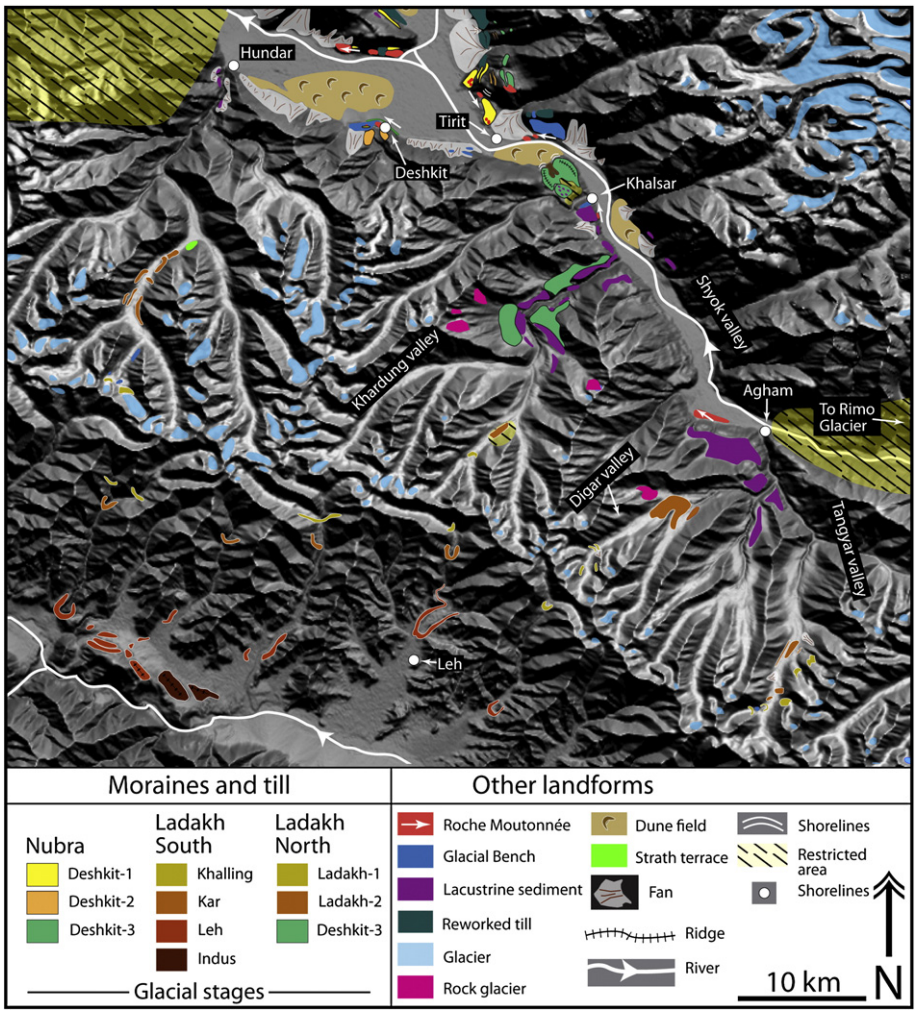

Fig. 3. Hillshade SRTM DEM showing the geomorphology of the Shyok Valley and the central Ladakh Range. The white arrows show the direction of ice movement based on erosional features on the roche moutonnées.

MELM method is not applied here because restricted access prevented the accurate mapping of lateral moraine deposits in the higher reaches of the Nubra Valley, and these cannot be easily seen on remote sensing imagery.

The mean values of the AAR, THAR, and AA methods are used in this study to estimate the contemporary ELA of Siachen Glacier, which has a thick debris cover. Ratios of 0.4 (AAR) and 0.5 (THAR) are used for the ELAs, because they have been shown to reflect the decreased melting in the ablation zone due to debris cover (Müller, 1980; Kulkarni, 1992; Seong et al., 2008). Standard values of 0.5 and 0.6 for the AAR method are also reported for easy comparison with other studies.

The AABR method is used to reconstruct former ELAs because it biases the mass balance in areas far above and below the ELA more than those close to the ELA (Osmaston, 2005). The area-altitudinal weighting is particularly important in the Karakoram due to the range's high relief. These former ELA reconstructions are considered estimates because of significant potential errors in estimating the area of the former glacier. These errors include uncertainty about the location of the former glacier terminus and the extent of the tributary glacial system. An iterative process was used to estimate the former tributary system, in which the glacial system's surface area was overestimated, the hypsometry was determined (cf. Dortch et al., 2009), and former ELAs were modeled using the mean of the AAR, THAR, and AA methods. The calculated mean former ELA and glacier extent were plotted in ArcMap 9.1. Tributaries that lay completely within the ablation zone (below the modeled ELA) were eliminated because they could not have had an accumulation zone and therefore would not have existed. This process was repeated until all the tributary glaciers contributed to the mass balance of the Deshkit 1 glacial stage glacier.

The AABR was calibrated to the average contemporary ELA (AAR 0.4, THAR 0.5, and AA methods) of Siachen Glacier to within 10 m. The calibrated AABR model was then used to estimate the former ELA for the Deshkit 1 glacial stage. The modeled AABR ELA is based on the contemporary glacier's parameters (structure of tributary system, percentage of debris cover, and balance ratio) and therefore the modeled Deshkit 1 glacial stage former ELA must follow a linear extrapolation of the current conditions. Departure from current parameters would make choosing the structure of tributary system, percentage of debris cover, and balance ratio somewhat arbitrary. The ELA depression (ΔELA) was determined by subtracting the reconstructed former AABR ELA from the modern AABR ELA.

Landform descriptions

Glacial landforms were delineated into three glacial stages on the basis of field mapping, relative position, elevation, and degree of weathering. Field mapping was undertaken during two two-month

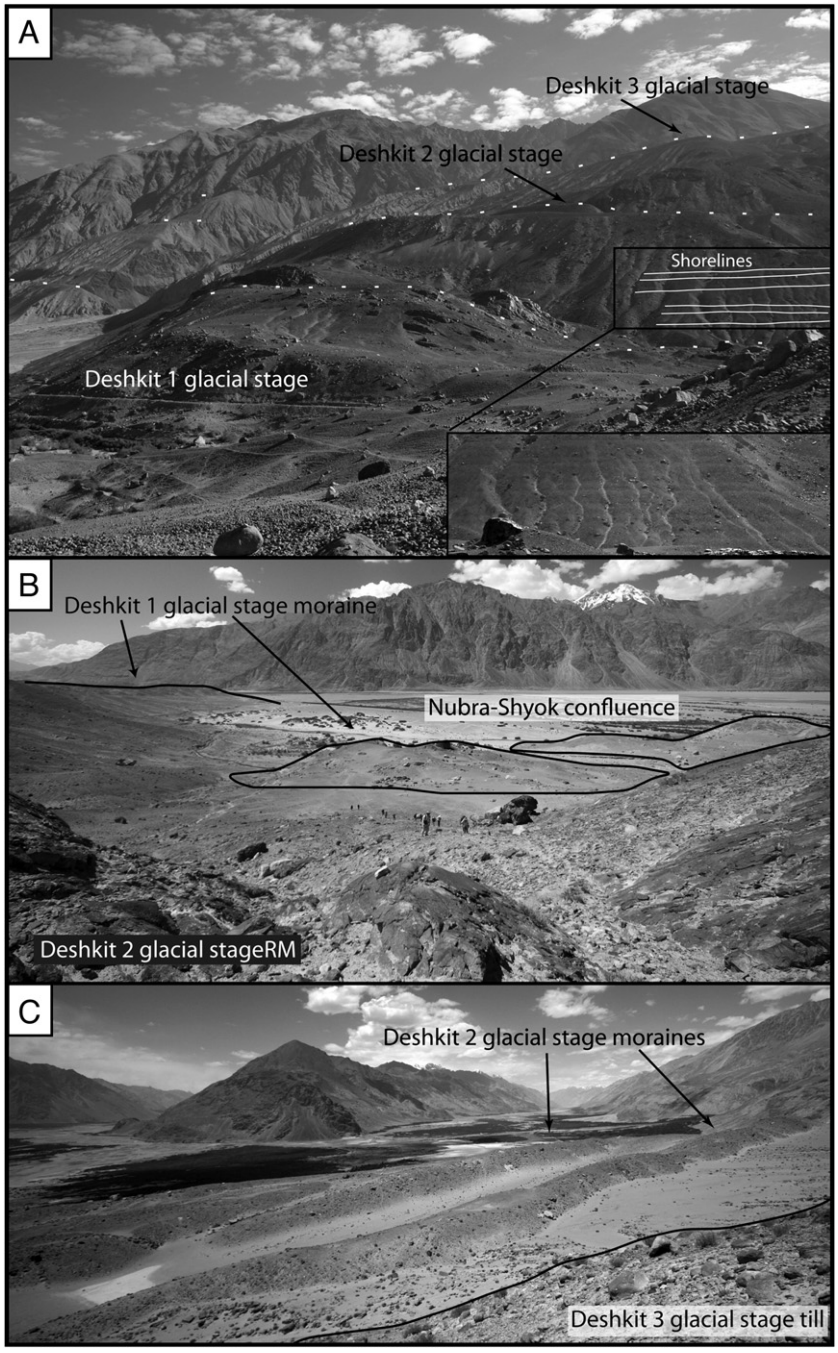

Fig. 4. Views of the large moraine complex near the village of Tirit. A) View looking northwards from ~1 km north of Trit village at the Karakoram showing moraines, roche moutonnées, and shorelines from the Deshkit 1, Deshkit 2, and Deshkit 3 glacial stages. The white dots represent boundaries between sediments of different glacial stages. B) View looking southwest from ~ 2 km north of Trit village of Deshkit 1 glacial stage moraines taken from on top of Deshiket 2 glacial stage roche moutonnées (RM). C) View looking west from ~1 km east of Trit village of the paired Deshkit 2 glacial stage moraines taken from Deshkit 3 glacial stage till slope. Black lines in B) and C) represent boundaries between sediments of different glacial stages.

field seasons using topographic maps, compass, and a handheld global positioning system (GPS).

Deshkit 3 glacial stage

Deposits from Deshkit 3 glacial stage are present throughout the Nubra, Shyok, and Khardung valleys (Figs. 2 and 4A). Near the village of Tirit, the Deshkit 3 glacial stage is represented by a moraine that comprises a large mass of cobbly till, which is located ~900 m above the valley floor (Figs. 4A and 5E). This deposit is denuded and contains no large boulders. Partially buried roche moutonnées protrude out of moraines. These were not sampled because the till cover is highly eroded and contains many small gullies.

Deshkit 3 glacial stage landforms are also located in the Shyok River valley near the village of Khalsar (Fig. 2B). These landforms trend northwest and comprise a composite three segments of lateral and lateral–frontal moraines and roche moutonnées with dark brown desert varnish. The lateral moraine from this deposit can be traced up the Khardung Valley, a tributary valley located in the Ladakh Range (Fig. 3). The Khalsar moraine was initially described by Phartiyal et al. (2005) as a landslide mass, but later reinterpreted by Pant et al. (2005) to be a lateral moraine. The moraine is composed of till capped by a ~20 m thick deposit of lacustrine sediment that consists of

Table 1
Locations, thickness, shielding, ^{10}Be ages, and surface conditions of samples collected in the Nubra and Shyok Valleys from this study (N/A - data not available). Details of Seong et al.'s (2007) Skardu glacial stage ^{10}Be ages (samples K2-1 through K2-9) recalculated using our methods are also shown.

Sample Name	Surface condition (cm)	Lithology	Latitude (°N)	Longitude (°E)	Elevation (m a.s.l.)	Thickness (cm)	Shielding correction	Uncorrected[a] ^{10}Be atoms ± error g^{-1} (10^6)	Corrected[b] ^{10}Be atoms ± error g−1 (10^6)	Age STD (ka)[c]	Age KN (ka)[d]	Age DZ (ka)[e]
NU-1	Polished, dark varnish, striations	Granodiorite	34.570	77.620	3237	3	1	3.342 ± 0.053	3.010 ± 0.048	81.7 ± 5.7	71.5 ± 4.6	64.0 ± 4.7
NU-2	1.0 cm exfoliation	Granitic	34.574	77.625	3247	1	1	2.696 ± 0.130	2.428 ± 0.117	64.2±5.4	56.3 ± 4.5	49.4 ± 4.3
NU-3	1.0 cm exfoliation	Granitic	34.574	77.625	3243	2	1	1.909 ± 0.073	1.719 ± 0.066	45.7 ± 3.6	40.1 ± 2.9	36.5 ± 3.0
NU-4	Polished, dark varnish, striations	Granodiorite	34.575	77.627	3293	1.5	1	3.308 ± 0.065	2.979 ± 0.058	77.3 ± 5.5	67.6 ± 4.4	60.4 ± 4.5
NU-5	Wind polished	Granitic	34.573	77.625	3243	1	1	1.943 ± 0.108	1.750 ± 0.097	46.2±4.1	40.5 ± 3.4	36.8 ± 3.4
NU-6	1.0 cm exfoliation	Granitic	34.574	77.626	3251	2	1	1.735 ± 0.085	1.563 ± 0.077	41.3 ± 3.5	36.9 ± 3.0	33.5±2.9
NU-7	0.2 cm disintegration	Granitic	34.545	77.638	3223	2	1	2.441±0.051	2.198 ± 0.045	59.4 ± 4.2	51.6 ± 3.4	45.7 ± 3.4
NU-8	0.2 cm disintegration	Granitic	34.545	77.638	3222	2	1	1.860 ± 0.045	1.675 ± 0.041	45.1 ± 3.2	39.7 ± 2.7	36.2 ± 2.7
NU-9	Fractured	Granitic	34.546	77.638	3223	3	1	1.006 ± 0.040	0.906 ± 0.036	24.5 ± 1.9	23.1 ± 1.7	21.0 ± 1.7
NU-10	Fractured	Granitic	34.546	77.638	3225	2	1	1.904 ± 0.058	1.715 ± 0.052	46.1 ± 3.4	40.4 ± 2.8	36.8 ± 2.9
NU-11	Striations	Granitic	34.546	77.638	3221	2	1	1.141 ± 0.048	1.028 ± 0.044	27.6±2.2	25.8 ± 1.9	23.4 ± 2.0
NU-12	Some polish	Granitic	34.547	77.637	3208	2.5	1	1.265 ± 0.046	1.140 ± 0.041	30.9 ± 2.4	28.6 ± 2.1	26.0 ± 2.1
NU-13	0.2 cm disintegration	Granitic	34.458	77.723	3552	2	1	5.545 ± 0.117	4.994 ± 0.106	113.9 ± 8.2	98.6 ± 6.5	86.0 ± 6.5
NU-14	0.2 cm disintegration	Gneiss	34.462	77.721	3542	3	1	5.211 ± 0.177	4.693 ± 0.160	108.4 ± 8.3	94.4 ± 6.8	81.9 ± 6.6
NU-15A	10 cm exfoliation	Gneiss	34.462	77.721	3534	3	1	1.651 ± 0.059	1.487 ± 0.053	33.8 ± 2.6	30.9 ± 2.2	27.4 ± 2.2
NU-15B	10 cm exfoliation	Gneiss	34.462	77.721	3534	3	1	1.771 ± 0.085	1.595 ± 0.077	36.3 ± 3.0	33.0 ± 2.6	29.1 ± 2.5
NU-16	0.2 cm disintegration	Granitic	34.462	77.720	3543	10	1	7.064 ± 0.271	6.363 ± 0.244	157.4 ± 12.6	132.5 ± 9.9	115.1±9.7
NU-17	0.2 cm disintegration	Granitic	34.462	77.720	3543	12	1	6.276 ± 0.139	5.653 ± 0.125	141.6 ± 10.3	119.7 ± 8.0	104.8 ± 8.0
NU-18	0.2 cm disintegration	Granitic	34.462	77.720	3543	12	1	4.783 ± 0.240	4.308 ± 0.217	107.0 ± 9.2	93.2 ± 7.6	80.8 ± 7.3
NU-19	0.2 cm disintegration	Granitic	34.462	77.720	3543	10	1	6.727 ± 0.540	6.059 ± 0.486	149.6 ± 162	126.1 ± 13.2	110.1 ± 12.5
NU-20	Polished, dark varnish, striations	Granitic	34.545	77.563	3277	2	0.72544	N/A	1.882 ± 0.056	68.1 ± 5.1	59.9 ± 4.2	52.6 ± 4.1
NU-21	Polished, dark varnish, striations	Granitic	34.545	77.563	3283	3	0.99002	N/A	3.102 ± 0.085	82.9 ± 6.1	72.5 ± 5.0	64.6 ± 5.0
NU-23	Polished, dark varnish, striations	Granitic	34.572	77.626	3245	2	0.99485	N/A	3.099 ± 0.078	83.5 ± 6.1	73.1 ± 4.9	65.3 ± 5.0
NU-24	Polished, dark varnish, striations	Granitic	34.572	77.626	3238	2	0.98925	N/A	3.927 ± 0.098	107.5 ± 7.9	93.9 ± 6.3	83.8 ± 6.4
NU-25	6.0 cm pit and 15 cm cavern	Granitic	34.574	77.626	3261	5	0.99463	N/A	1.652 ± 0.055	44.8 ± 3.4	39.5 ± 2.8	35.9 ± 2.8
NU-26	1 cm disintegration	Granitic	34.574	77.626	3253	4	0.97991	N/A	1.771 ± 0.090	48.6 ± 4.1	42.3 ± 3.4	38.4 ± 3.4
NU-27	Polished, dark varnish	Volcanic	34.458	77.723	3554	5	0.97991	N/A	5.023 ± 0.144	119.9 ± 9.0	103.1 ± 7.1	90.5 ± 7.1
NU-28	2 cm pit	Granitic	34.458	77.723	3556	3	0.99087	N/A	5.018 ± 0.107	116.3 ± 8.4	100.4 ± 6.6	87.8 ± 6.7
NU-29	10 cm pit and 75 cm cavern	Granitic	34.458	77.723	3557	4	0.98944	N/A	5.824 ± 0.143	136.9 ± 10.1	116.2 ± 7.8	101.7 ± 7.9
NU-30	Fresh	Granitic	34.458	77.723	3556	3	0.98944	N/A	5.466 ± 0.119	126.0 ± 9.1	107.8 ± 7.2	94.7 ± 7.2
K2-1	N/A	N/A	35.315	75.626	2598	3	1	3.490 ± 0.110	3.143 ± 0.099	124.1 ± 9.4	107.8 ± 7.6	101.8 ± 8.1
K2-2	N/A	N/A	35.314	75.625	2601	3	1	4.650 ± 0.070	4.188 ± 0.063	166.9 ± 11.9	143 ± 9.3	133.6 ± 10.0
K2-3	N/A	N/A	35.314	75.625	2611	3	1	3.860 ± 0.090	3.477 ± 0.081	136.6 ± 10.0	117.6 ± 7.9	110.8 ± 8.5
K2-4	N/A	N/A	35.315	75.623	2598	2	1	4.710 ± 0.090	4.242 ± 0.081	168.0 ± 12.2	144.1 ± 9.5	134.5 ± 10.2
K2-5	N/A	N/A	35.314	75.626	2602	3	1	2.940 ± 0.050	2.648 ± 0.045	103.8 ± 7.3	91.7 ± 5.9	86.3 ± 6.4
K2-6	N/A	N/A	35.314	75.627	2613	2	1	4.020 ± 0.110	3.621 ± 0.099	141.1 ± 10.5	121.1 ± 8.3	114.0 ± 8.9
K2-7	N/A	N/A	35.317	75.621	2545	2	1	2.530 ± 0.060	2.279 ± 0.054	91.5 ± 6.6	81.0 ± 5.4	76.4 ± 5.8
K2-8	N/A	N/A	35.318	75.618	2557	3	1	3.100 ± 0.070	2.792 ± 0.063	112.8 ± 8.2	99.0 ± 6.6	93.9 ± 7.1
K2-9	N/A	N/A	35.318	75.617	2557	3	1	1.910 ± 0.050	1.720 ± 0.045	68.7 ± 5.0	61.2 ± 4.1	57.7 ± 4.4

Notes-
Assume zero erosion rate, standard pressure, and $\rho = 2.7\ g/cm^3$ for all samples. PRIME Laboratory AMS was calibrated using KN Standard Be 0152 with a $^{9}Be/^{10}Be$ ratio of 8.558×10^{-12} atoms (c.f. Nishiizumi et al., 2007).

[a] ^{10}Be concentrations and error of samples measured before January 2007.

[b] ^{10}Be concentrations and error of samples corrected to KN Standard Be 0152 and samples measured after January 2007 (Nishiizumi et al., 2007).

[c] Age calculated using scaling model of Stone (2000) scaling scheme.

[d] Age calculated using scaling model of Nishiizumi et al. (1989) scaling scheme.

[e] Age calculated using scaling model of Desilets and Zreda (2003) scaling scheme.

cm-scale clay rhythmites (Pant et al., 2005). We confirmed in the field that this deposit is a moraine based on its sedimentology and morphology; distinct ridges composed of diamict with edge rounded glacially faceted clasts and are interpreted as lateral and lateral–frontal moraines with steep sides that that have not undergone gravitational reworking.

The Karakoram tributary valleys were not mapped in detail due to restricted access. Besides Deshkit 3 glacial stage moraines, no other moraines were found in the Shyok Valley between the Nubra–Shyok confluence and the Tangyar–Shyok confluence (Fig. 3). However, a set of west-oriented roche moutonnées is located farther up the Shyok valley, west of Agham village (Figs. 3 and 5F). These roche moutonnées are granitic, exfoliated, with patchy rock varnish. Based on weathering criteria, we correlate these roche moutonnées to the Deshkit 3 glacial stage. Deshkit 3 roche moutonnées located near Khalsar and a second set on the edge of an alluvial fan east of Tirit have dark brown patchy rock varnish and occasional glacially polished surfaces (Figs. 2B, 5D and E). These roche moutonnées are heavily fractured and have undergone extensive physical weathering (exfoliation and frost wedging).

Surface boulders on the Deshkit 3 moraine near the village of Khalsar are abundant and range in size from 0.5 to ≥2 m in diameter and are ~1.0 m tall. These boulders (NU-28 to NU-30) exhibit up to 10 cm-high knobs produced by disintegration of the boulder surfaces. Some boulders exhibit cavernous weathering with pits up to 0.75 m deep on their sides. Large cobbles, 10–12 cm in diameter, are also present on the moraine surface. These cobbles are well inset into the moraine surface and have weathering pits up to 2 mm deep. Samples were collected from surface boulders (NU-13 to NU-15), surface cobbles (NU-16 to NU-19, NU-28), and roche moutonnées near Khalsar (NU-27) that are associated with the moraine in the Shyok River valley (Fig. 2B).

Deshkit 2 glacial stage

Deshkit 2 glacial stage landforms are represented by two moraines and several roche moutonnées occurring up to ~420 m above the present valley floor at Nubra–Shyok confluence (Figs. 2, 4A and C). These paired moraines can be traced up the Nubra Valley for ~15 km (Fig. 2). The moraines comprise till with occasional granitic surface boulders ≥4 m in diameter. Evidence of exhumation/toppling was readily apparent; boulders were unburied and in unstable positions on moraine crests. Unfortunately, we could not find any boulders suitable for sampling. However, roche moutonnées (3240–3300 m a.s.l.) at this location featured polished/striated surfaces, were clear of debris, had dark brown desert varnish, trend southeast, and were suitable for sampling (Fig. 5B). In contrast, Deshkit 3 glacial stage roche moutonnées are heavily fractured and have undergone extensive physical weathering (exfoliation and frost wedging) (Figs. 5D and E). The amount of rock eroded to produce Deshkit 2 glacial stage roche moutonnées can be estimated from the vertical faces on their leeward ends, where glacial plucking had created steps in the bedrock with polished surfaces. The leeward steps of Deshkit 2 glacial stage roche moutonnées indicates

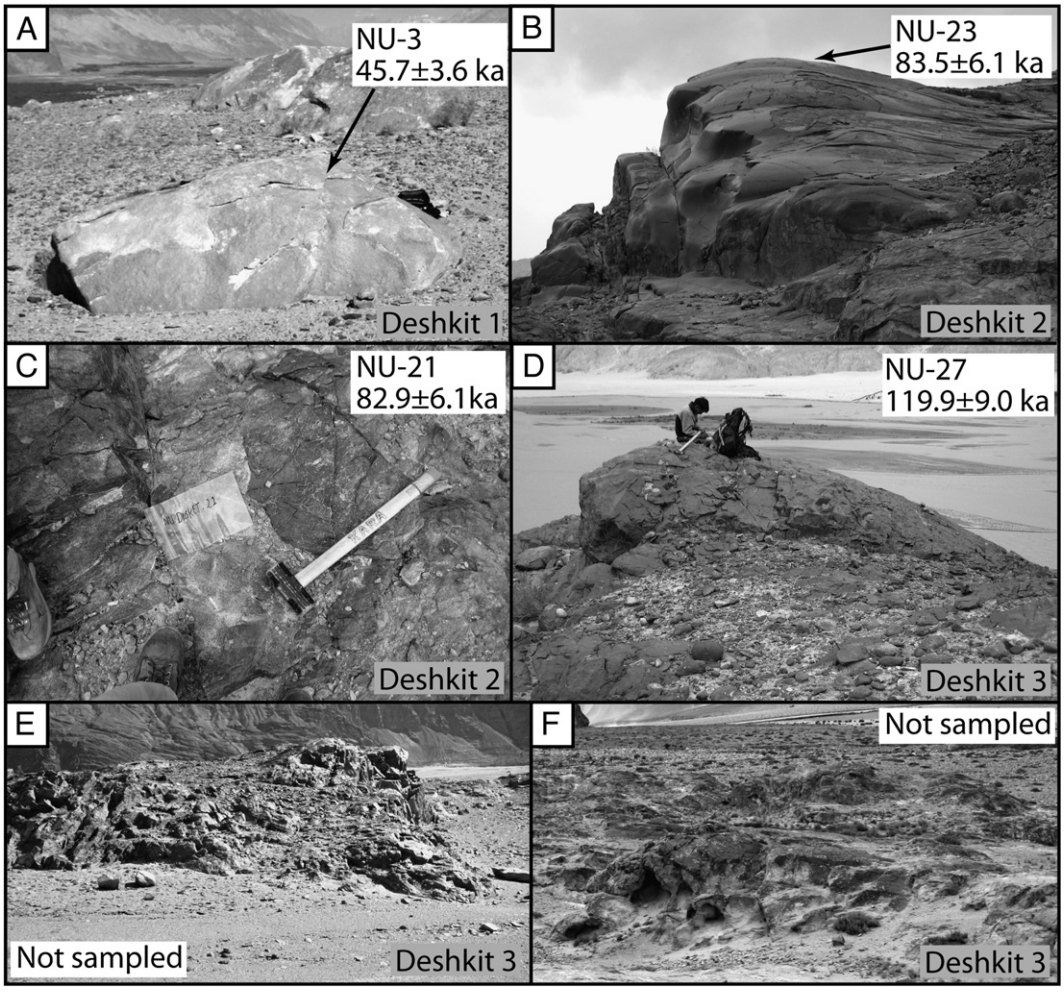

Fig. 5. Views of typical sampling locations for ^{10}Be terrestrial cosmogenic nuclide surface exposure dating (name of glacial stages highlighted in bottom right hand corner of each photograph). A) Boulder on the crest of the Deshkit 1 glacial stage moraine (~3 m long). B) View looking southwest at a Deshkit 2 glacial stage roche moutonnée located north of the Tirit Moraine (~6–7 m tall). C) Plucked surface of a Deshkit 2 glacial stage roche moutonnée located near the village of Deshkit. D) View looking northeast at a Deshkit 3 glacial stage roche moutonnée near the village of Khalsar. The hammer in C) and D) is 50 cm long. E) and F) Deshkit 3 glacial stage roche moutonnées located east of the village of Tirit and west of the village of Agham, respectively. The field of view for E) and f) is ~150 m. Note the degree of weathering on Deshkit 3 glacial stage roche moutonnées as compared to Deshkit 2 glacial stage roche moutonnées.

≤7 m of bedrock plucking, which would have removed any significant ^{10}Be inheritance.

Samples NU-1, NU-4, and NU-23 were collected from the crest of roche moutonnées and sample NU-24 from a plucked surface. Roche moutonnées at approximately the same elevation (~3275 m a.s.l.) are also located near the village of Deshkit (Fig. 2B). These roche moutonnées are glacially polished, clear of surface debris, have striations and mini-crag and tail and mini-roche moutonnées features trending northeast, and show evidence of ≥5 m of glacial plucking on their leeward side. Samples NU-20 and NU-21 were collected from plucked surfaces on these roche moutonnées.

There is no evidence of former glaciers from the Karakoram or Ladakh Range tributary valleys advancing into the Nubra or Shyok valleys during the Deshkit 2 glacial stage. Moreover, there are no Deshkit 2 glacial stage deposits in the mapped extent of the Shyok valley up to the confluence with the Tangyar valley (Fig. 3).

Deshkit 1 glacial stage

The main Deshkit 1 glacial stage moraine is a ~135-m-tall nearly continuous ~1 km-long ridge that declines eastward to an ~80-m-high hummocky lateral–frontal moraine (Fig. 4B). The moraine is located on the east side of the Nubra valley near the village of Tirit and can be traced up the Nubra Valley for ≥30 km (Fig. 2). The hummocky deposits are oriented southwest–northeast and curve south near the mouth of the Shyok River valley. The southward-declining elevation and morphology of the moraine suggests that it represents the westward limit of Deshkit 1 glacial stage. The moraine blocks a tributary valley, whose stream has dissected the moraine and has reworked it to form an alluvial fan (Pant et al., 2005). The fluvially incised moraine ridges indicate that tributary glaciers from the southern side of the Karakoram did not extend to the Nubra–Shyok confluence during this glacial stage.

The Deshkit 1 moraine near Tirit is composed of till with numerous granitic surface boulders 1–2 m in diameter and 0.5–1.2 m high (Fig. 5A). Many of the boulders have wind polished surfaces (NU-5). Other boulders are exfoliated (NU-2, NU-3, and NU-6), with granular weathering features (NU-26), are fractured (NU-9 and NU-10), or have weathering pits ≥6 cm deep (NU-25). This moraine onlaps the edge of the Deshkit 2 glacial stage roche moutonnées (Fig. 4A). Samples NU-2 and NU-3, NU-5 to NU-12, NU-25, and NU-26 were collected from boulders on this moraine.

The moraines and roche moutonnées of the Deshkit 1 and Deshkit 2 glacial stages, located near the village of Deshkit, indicate that Siachen Glacier flowed down the Nubra valley, turning northwest at the Nubra–Shyok confluence (Fig. 2b). The contemporary drainage follows the same path. There are no morphostratigraphically correlative glacial deposits for the Deshkit 1 glacial stage in the mapped portion of the Shyok Valley from Rimo Glacier, transverse glaciers of the Karakoram, or glaciers from the Ladakh Range (Fig. 3). The declining elevation of deposits in the confluence suggests that the Deshkit 1 glacial stage terminated near the village of Hundar (Fig. 3).

Shorelines

Wave-cut shorelines from 3150 to 3290 m a.s.l. are present in Deshkit 2 glacial stage till, adjacent to, but outside the limit of the Deshkit 1 moraine (Fig. 4A). Another set of shorelines are eroded into Deshkit 3 glacial stage till from 3220 to 3350 m a.s.l. near Khalsar (Fig. 2B). This morphostratigraphy indicates that the formation of the shorelines occurred after the culmination of the Deshkit 2 glacial stage and before the Deshkit 1 glacial stage. Samples were not collected from these shorelines for ^{10}Be dating.

Ages of landforms

^{10}Be exposure ages for each landform are listed in Table 1 and plotted in Fig. 6. These ages were examined using the mean square of weighted deviates (MSWD) method of McDougall and Harrison (1999) to help assess whether they statistically represent a single population or event. Outliers were removed iteratively from the dataset. This process was repeated until the MSWD was at or near 1. We use the

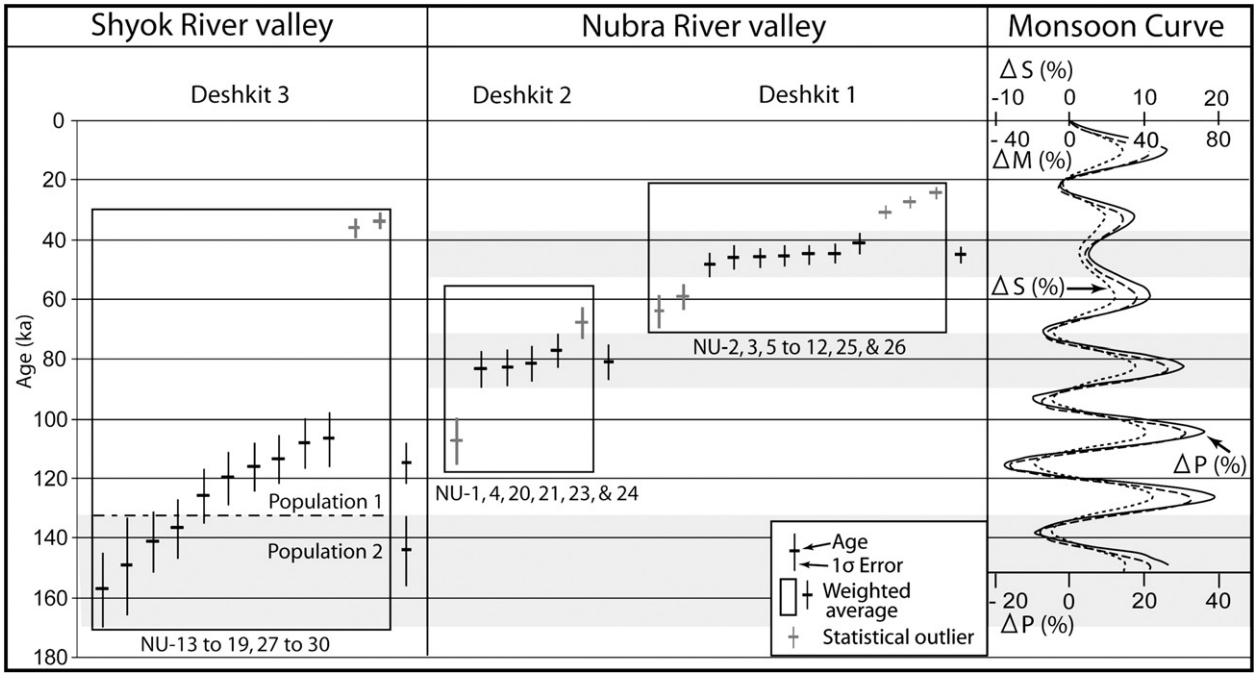

Fig. 6. Plot of ^{10}Be terrestrial cosmogenic nuclide surface exposure ages for the study area. Ages are grouped (boxed) by glacial stage in descending age. Gray bars represent glacial stages defined by the maximum error of samples in a single population. Horizontal dashed line distinguishes the two age populations identified using the MSWD method. Prell and Kutzbach (1987) simulated monsoon pressure index (Δ*M* percentage, dashed line) for the Indian Ocean, simulated changes in precipitation (*P* percentage, black line) in southern Asia, and variations in Northern Hemisphere solar radiation (Δ*S* percentage, dotted line).

Table 2
Position and aspect of glacier morphology, and ELAs.

Glaciers	Toe (m a.s.l.)	Headwall (m a.s.l.)	Aspect	Change in contour direction (m a.s.l.)	AAR-0.4 (m a.s.l.)	AAR-0.5 (m a.s.l.)	AAR-0.6 (m a.s.l.)	THAR-0.5 (m a.s.l.)	AA (m a.s.l.)	Mean ± stdev (m a.s.l.)	AABR ratio	AABR value (m a.s.l.)	ELA depression (m a.s.l.)
Siachen Glacier	3700	7300	SW	5200-5400	5580	5450	5250	5500	5460	5510 ± 60	0.8	5500	N/A
Disket stage 1	3100	7300	SW	N/A	5470	5340	5200	5200	5150	5270 ± 170	0.8	5210	~290
Disket stage 2[a]	N/A	7300	SW	N/A	N/A	N/A	N/A	N/A	N/A	N/A	0.8	N/A	N/A
Disket stage 3[a]	N/A	7300	SW	N/A	N/A	N/A	N/A	N/A	N/A	N/A	0.8	N/A	N/A

Notes-
[a] Unable to calculate AAR, THAR, AA, or AABR because the extent of glaciation is unknown.

weighted mean and standard error (M_w) of the MSWD population to define the ages of landforms because the precisions of the age determinations differ and therefore more precise ages are weighted more heavily. Using the MSWD method, NU-2, NU-7, NU-9, NU-11, NU-12, NU-15A, NU-15B, NU-20 and NU-24 were eliminated from the data set and are not considered further in our analysis (Fig. 6). Approximately 10% of the samples likely have inherited ^{10}Be and about 20% have ages significantly younger than the clustered ages. Moraine ^{10}Be ages are referred to as deglaciation ages as moraine boulders are likely exhumed or toppled until early stabilization is reached sometime after deglaciation (Briner et al., 2005; Dortch et al., 2008).

After removal of outlier ages, boulder samples from the Deshkit 3 glacial stage moraines have ^{10}Be ages that range from ~107 ka to ~157 ka (Table 1). These ages cluster into two distinct age populations at an M_w of 115 ± 7 ka with a MSWD of 0.53 (NU-13, NU-14, NU-18, NU-27, NU-28, NU-30) and an M_w of 145 ± 12 ka with a MWSD of 0.45 (NU-16, NU-17, NU-19, and NU-29) (Fig. 6). The spread in ^{10}Be ages is likely due to surface weathering. Weathering characteristics such as the ≤0.75 m deep caverns and surface disintegration can be accounted for by a 4.2 m Ma^{-1} boulder surface erosion rate. The roche moutonnées, which lie below lacustrine and till deposits on a steep slope, have likely been exhumed. In such cases, the oldest age population is likely the most accurate representation of the true age of the landform (cf. Briner et al., 2005). Therefore, we suggest the M_w age of 145 ± 2 ka as the lower limit of deglaciation for the Deshkit 3 glacial stage.

After removal of outliers, Deshkit 2 roche moutonnée samples have ^{10}Be ages that date to ~82 to 84 ka (NU-1, NU-21, and NU-23) on the north side and ~77 ka (NU-4) on the southern side of the Nubra–Shyok confluence (Fig. 6, Table 1). These roche moutonnées, top and plucked surfaces, have a combined M_w age of 81 ± 6 ka with MWSD of 0.19. The leeward side of these roche moutonnées indicates glacial plucking of >5 m of bedrock. Therefore, significant TCN inheritance is unlikely. Accounting for an erosion rate of 4.2 m Ma^{-1} could push the M_w age of 81 ± 6 ka to ~100 ka. The preservation of striations indicates that surface erosion since deglaciation has been minimal, but this could also indicate recent exhumation, which would underestimate its age. Therefore, we suggest an age of 81 ± 6 ka for the Deshkit 2 glacial stage is reasonable.

After removal of outliers, Deshkit 1 glacial stage boulder samples (NU-3, NU-5, NU-6, NU-8, NU-10, NU-25, and NU-26) display ^{10}Be ages that range from ~45 to 49 ka (Fig. 6, Table 1). These ages cluster well with an M_w age of 45 ± 3 ka and a MWSD of 0.30. The low MWSD and tight clustering of ^{10}Be ages on the Nubra moraine suggest a minimum age of ~45.2 ± 2.7 ka for the Deshkit 1 glacial stage.

ELA reconstructions

Contemporary ELA

The AAR (0.4) gives the highest ELA at 5580 m a.s.l., while the THAR (0.5) is in the middle of the range (5500 m a.s.l.) and the AA (5460 m a.s.l.) method gives the lowest value (Table 2). Following the suggestion of Benn et al. (2005) we use the average of the AAR (0.4), THAR (0.5), and AA methods for the modern ELA's and use 1σ for error, which yields an ELA estimate of 5510 ± 60 m a.s.l. for the contemporary Siachen Glacier (Figs. 7A, Table 2). The low 1σ shows that the three methods agree well. Approximately 80% of the surface area for Siachen Glacier has a low gradient with ~60% of the glacier surface area within the ablation zone (Fig. 7B). This is likely the result of the insulating effects of thick a debris-cover.

Former ELA reconstruction

Calibration of the AABR model to the modern ELA values gives a ratio of 0.8. Low AABR ratios (~ 1.0), however, are expected for debris-covered glaciers (Osmaston, 2005). The reconstructed hypsometric curves used to bin elevations and calibrated the AABR model is shown in Figure 7B and Table 2.

The extent of the Deshkit 1 glacial stage is relatively well defined by deposits near the village of Hundar (Figs. 3 and 7A). The downvalley extent of glaciers for the Deshkit 2 and Deshkit 3 glacial stages are unknown and therefore ELA reconstructions were not undertaken for these glacial stages. The AABR-modeled ELA is 5210 m a.s.l. and is graphically represented in Figure 7B. The mean and 1σ of the AAR (0.4), THAR (0.5), and AA methods is 5270 ± 170 m a.s.l. The mean former ELA is higher and has more error than the AABR-modeled ELA. This is due to the AAR (0.4) method (5470 m a.s.l.). Osmaston (2005) suggested the AA (5150 m a.s.l.) method typically yields more reliable results than the AAR method. Moreover, the THAR (0.5 at 5200 m a.s.l.) and the AA methods agree well with the AABR model. Therefore, we use the AABR method to define the ΔELA (~290 m).

Discussion: synchroneity and extent of glaciation

Deshkit 3 glacial stage

Determining the extent of glaciation during the Deshkit 3 glacial stage (M_w of 145 ± 12 ka) is difficult due to the absence of terminal moraines (Figs. 2 and 3). The northwest trend of roche moutonnées and the dated moraine section near Khalsar village indicated that glacial ice was flowing westward in the Shyok Valley toward the Nubra–Shyok confluence. This moraine near Khalsar village, which can be traced up the Khardung Valley, is the morphostratigraphic equivalent of the Leh Glacial stage moraines described by Owen et al. (2006) on the southern side of the Ladakh Range (Fig. 3).

The west trend of the roche moutonnées near the Tangyar–Shyok confluence suggests that they were formed by Rimo Glacier and/or glaciers from Tangyar or Digar valleys (Ladakh Range tributary valleys). Neither Rimo Glacier, glaciers located up-valley of the roche moutonnées, or glaciers from the Tangyar or Digar valleys could have advanced to the Nubra–Shyok confluence without eroding

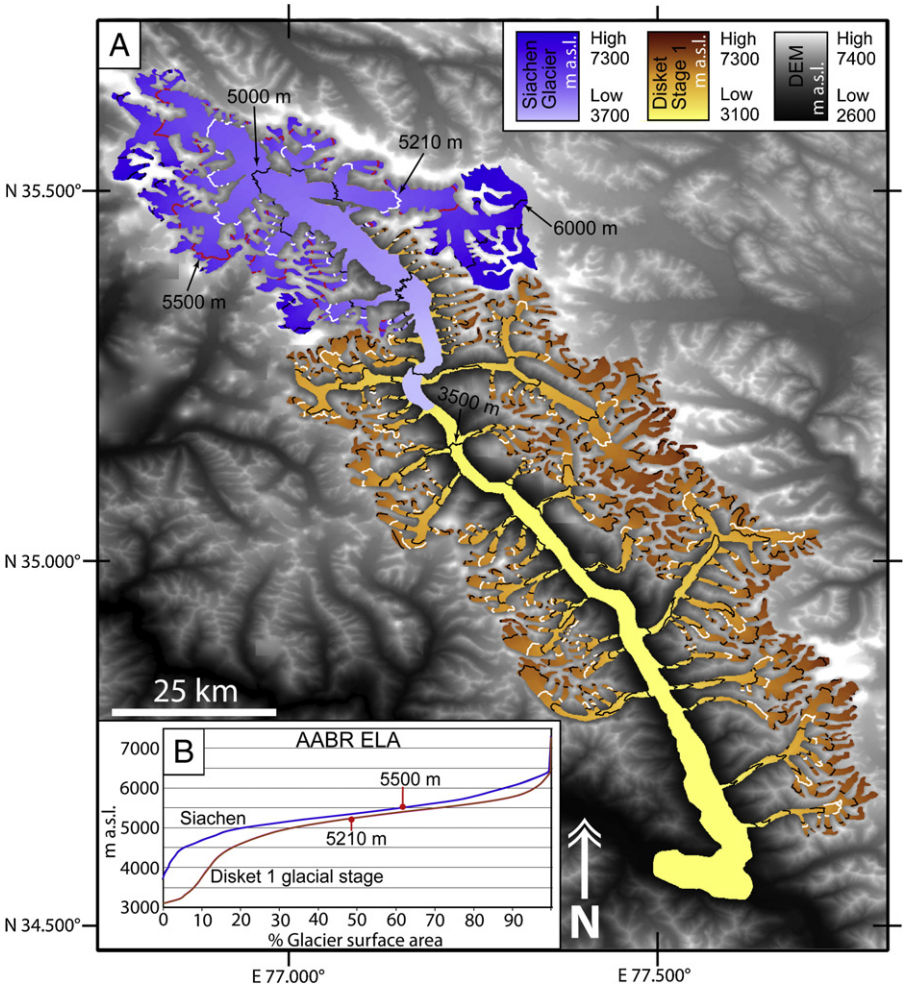

Fig. 7. SRTM DEM of the contemporary Siachen and Deshkit 1 stage glacial systems in the Nubra valley. Modern ELA's are marked by red and Deshkit 1 glacial stage marked by white contours. Contour interval is 500 m (black lines). B) Hypsometric curves for the contemporary Siachen Glacier and reconstructed for the Deshkit 1 glacial stage. The ELAs were determined using the AABR method and are marked on the hypsometric curves.

the roche moutonnées near Agham village (Fig. 3). It is likely that glaciers from these sources contributed to the Deshkit 3 glacial stage deposits. However, the preservation of the Deshkit 3 glacial stage roche moutonnées suggests that glaciers from these sources did not advance to the Nubra–Shyok confluence during subsequent glacial stages.

Correlative deposits in the Nubra valley show that Siachen Glacier also reached the village of Deshkit, ~100 km from its present position. Glacial sediments of the Deshkit 3 glacial stage are ~760 m higher than those for the Deshkit 1 glacial stage in the Nubra–Shyok confluence. The plug of sediment in the Shyok Valley near Khalsar (Fig. 2) indicates Siachen Glacier likely blocked or stalled the Shyok trunk glacier, resulting in the development of large and well-formed composite moraines near the village of Khalsar.

Seong et al. (2007) suggested that Biafo, Panmah, and Baltoro Glaciers in the Central Karakoram of northern Pakistan advanced synchronously during the Skardu glacial stage at MIS-6 (>150 km). Recalculation of Seong et al. (2007) ^{10}Be ages using our methods results in the removal of 3 outliers. Using the MSWD method gives M_w ages of 112 ± 10 ka and 157.0 ± 13.0 ka with statistical indicators of 0.97 and 1.26, respectively (Fig. 8, Table 1). The statistical indicator is high but values at or near one are acceptable (McDougall and Harrison, 1999). As with the Deshkit 3 glacial stage ages, the oldest age population represents the best minimum age approximation.

The Skardu glacial stage M_w age of 157 ± 13 ka has >50% overlap of error with the Deshkit 3 glacial stage M_w age at 145 ± 12 ka. However, the older MSWD populations in both the Disket 3 and Skardu glacial

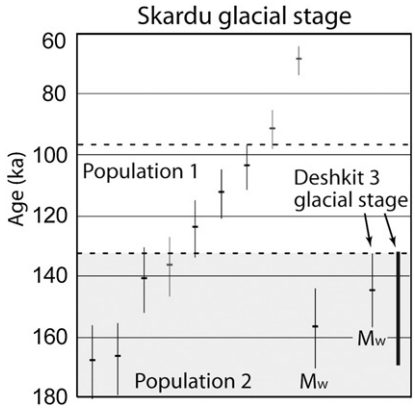

Fig. 8. Plot of recalculated ^{10}Be terrestrial cosmogenic nuclide surface exposure ages from Seong et al. (2007) for the Skardu glacial stage. Ages are plotted in descending age. Horizontal dashed line distinguishes the two age populations identified using the MSWD method. The Deshkit 3 glacial stage M_w age (144.5 ± 12.0 ka) and population-2 are plotted for reference.

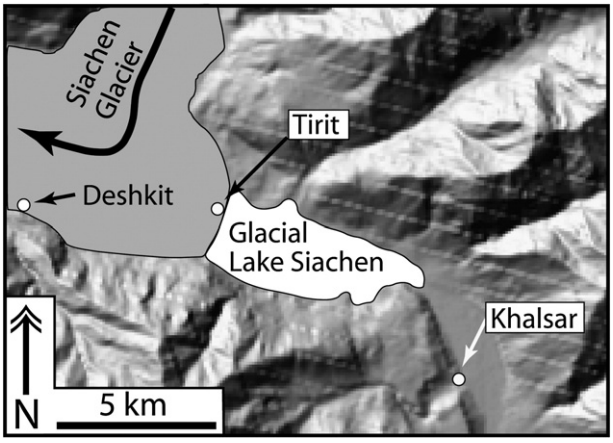

Fig. 9. Hillshade SRTM DEM showing the reconstructed extent of Glacial Lake Siachen during the Deshkit 2 glacial stage. The paleolake extent was determined by intersecting a plane at the elevation of the highest shoreline (3350 m a.s.l.) with the hillshade DEM in ArcMap 9.1.

stage datasets have 100% overlap (Fig. 8). The difference in M_w ages of the Deshkit 3 and Skardu glacial stages may be due to multiple glacial advances within each glacial cycle or differences in boulder weathering rates between areas. These glacial stages likely represent the local maximum glacial extent in the Karakoram and Ladakh Range during MIS-6. Within the error of ^{10}Be dating, there is synchroneity on Milankovitch timescales of glaciation in both the Karakoram and northern side of the Ladakh Range during MIS-6. The extent of the Skardu glacial stage in the Central Karakoram of northern Pakistan is similar to the Deshkit 3 glacial stage extent, where glaciers advanced >100 km. However, glaciers in the Khardung Valley (Ladakh Range) only advanced ~33 km from their present positions during MIS-6 (Fig. 2). The large error associated with the age of Deshkit 3 glacial stages does not allow us to resolve whether it occurred during insolation maxima or minima, or their precise position on Prell and Kutzbach's (1987) modeled monsoon intensity curve (Fig. 6).

Deshkit 2 glacial stage

Determining the extent of glaciation during the Deshkit 2 glacial stage (M_w of 81 ± 6 ka) is difficult due to the absence of terminal moraines (Fig. 2B). Glacial sediments from Deshkit 2 glacial stage are ~260 m higher than Deshkit 1 glacial stage sediments in the Nubra–Shyok confluence. This difference shows that glacial ice was thicker and, therefore, more extensive than the Deshkit 1 glacial stage (~100 km). The preserved Deshkit 3 glacial stage glacial landforms in the Shyok valley preclude glaciers sourced on the northeast side of the Karakoram, such as Rimo Glacier, from advancing into the Nubra–Shyok confluence during the Deshkit 2 glacial stage. Morphostratigraphically equivalent moraines in Ladakh Range tributary valleys are on average 15.4 ± 3.4 km up-valley from their confluence with the Shyok valley or 9.2 ± 1.6 km from the contemporary cirque glaciers (Fig. 3). The difference in glacial extent between Siachen Glacier (≥100 km) and glaciers on the northern side of the Ladakh Range may be due to a variety of factors, including elevation, catchment area, precipitation differences, relief, and glacier aspect. Moreover, there is no evidence (till, roche moutonnées or moraines) of glaciers advancing out of the south facing Karakoram tributaries during Deshkit 2 glacial stage time. Therefore, the Deshkit 2 glacial stage landforms in the Nubra valley were solely produced by Siachen Glacier.

Owen et al. (2008) shows general synchroneity of glaciation during late MIS-5/early MIS-4. The Deshkit 2 glacial stage correlates with the more extensive late MIS-5/early MIS-4 glaciation that is recognized in most of the monsoon dominated regions. However, glacial deposits correlative to the Deshkit 2 glacial stage have not been discovered in the Central Karakoram of northern Pakistan. This may be due to the lack of preservation or it could represent asynchronous glaciation due to Siachen Glacier being more heavily influenced by the monsoon than Baltoro Glacier region. The large error associated with the age of Deshkit 2 glacial stage do not allow us to resolve whether it occurred during insolation maxima or minima, or their precise occurrence on Prell and Kutzbach's (1987) modeled monsoon intensity curve (Fig. 6).

The overlap of shoreline elevations, 3150 to 3290 m a.s.l. near Tirit and from 3220 to 3350 m a.s.l. near Khalsar, suggests that they were formed contemporaneously. Reconstructions of the former lake extent using the highest shoreline show that the lake extended from Tirit to the Deshkit 3 moraine near Khalsar (Fig. 9). Based on the current elevation of the Nubra–Shyok confluence (3115 m a.s.l.) and the highest shoreline (3350 m a.s.l.) the deepest part of the paleolake was ~235 m at the ice proximal end, near Tirit. This is a maximum estimate as glacial and fluvial erosion since the Deshkit 2 glacial stage may have lowered the elevation of the Nubra–Shyok confluence to its contemporary elevation of 3115 m a.s.l. Blocking the Nubra River would not allow the formation of the shorelines near the village of Khalsar because they would be located on the down-stream side of the valley. Therefore, these shorelines necessitate that the Shyok River was obstructed. We suggest that Siachen Glacier blocked the Shyok River and created a glacially dammed lake (which we call Glacial Lake Siachen) during the Deshkit 2 glacial stage (Fig. 9).

The elevation of the highest shoreline (3350 m a.s.l.) is well above the crest of the Deshkit 1 glacial stage moraine (3260 m a.s.l.). The lateral moraines for the Deshkit 2 glacial stage are 3420 m a.s.l. and glacial ice could have easily blocked the Shyok River and led to lake formation. The shorelines inset into Deshkit 2 till near Tirit must have formed during the deglaciation of the Deshkit 2 glacial stage when fresh till at the lake margin was exposed to erosive wave action. This would account for the lack of higher shorelines for Glacial Lake Siachen near Tirit as compared to the shorelines inset into Deshkit 3 till near Khalsar, which were likely exposed to erosive wave action during the entire existence of Glacial Lake Siachen. The presence of the lower shorelines (3150 m a.s.l.) suggests that the initial drainage of Glacial Lake Siachen was slow during the deglaciation of Deshkit 2 glacial stage at ~81 ka.

Deshkit 1 glacial stage

The rapidly declining elevation of Deshkit 1 moraines in the Nubra–Shyok confluence indicated that glacial ice terminated near the village of Hundar, which gives a glacial extent of ~100 km from the contemporary snout of Siachen Glacier. The Deshkit 3 roche moutonnées in the Shyok Valley and Deshkit 2 moraines in the Ladakh Range preclude glacier contribution from these sources during the Deshkit 1 glacial stage. Morphostratigraphically equivalent moraines in Ladakh Range tributary valleys are on average 22.0 ± 4.7 km up-valley from the confluence with the Shyok valley or 2.7 ± 0.6 km from their contemporary cirque glaciers (Fig. 3). In addition, there is no evidence of Karakoram tributary glaciers advancing into the Shyok Valley during this time. There is a significant difference in glacial extent between Siachen Glacier (~100 km) and glaciers on the northern side of the Ladakh Range (2.7 ± 0.6 km). In addition, there is no evidence of glaciers advancing out of the Karakoram tributaries. The Deshkit 1 glacial stage landforms in the Nubra–Shyok confluence could have only been deposited Siachen Glacier.

Seong et al. (2007) documented and dated the Mungo (12–16 ka, ~80 km extent), and the Askole (~5 ka, 20 km extent) glacial stages in the Central Karakoram. Correlative glacial deposits to the Mungo and Askole glacial stages have not been found in the Nubra and Shyok valleys. The region between Deshkit 1 glacial stage landforms and the snout of Siachen Glacier are inaccessible and we were unable to map

it, however no glacial landforms younger than Deshkit 1 glacial stage were recognized on remote sensing imagery. Moreover, glacial deposits correlative to the Deshkit 1 glacial stage (M_w of 45 ± 3 ka) have not been discovered in the Central Karakoram of northern Pakistan. This may be due to the lack of preservation, or it could represent asynchronous glaciation. It is unlikely the monsoon was responsible for asynchroneity, as the Deshkit 1 glacial stage (45 ± 3 ka) likely occurred during a time of weak simulated monsoon pressure and precipitation (Prell and Kutzbach (1987; Fig. 6).

Owen et al. (2008) suggest broad synchroneity of glacial maxima during MIS-3 in many regions across the Himalayan mountain belt. The Deshkit 1 glacial stage, therefore, follows the temporal pattern of glaciation that is recognized in most of the monsoon dominated, Transhimalaya, and westernmost Tibetan regions.

Conclusions

Glacial landforms for three glacial stages date to ~45 ka (Deshkit 1 glacial stage), ~81 ka (Deshkit 2 glacial stage) and ~145 ka (Deshkit 3 glacial stage). Within error of ^{10}Be dating, the Deshkit 1 and 2 glacial stages show synchroneity of glaciation with regions primarily controlled by monsoon precipitation during MIS-3 and the MIS 5/6 transition, respectively (cf. Owen et al., 2008). The timing of glaciation across the Central Karakoram and Ladakh Range during MIS-6 is synchronous on Milankovitch timescales (and within error of each other), with the Deshkit 3 glacial stage dating to 145 ± 12 ka (M_w) in the Nubra, Shyok and Khardung Valleys (Ladakh Range) and the recalculated ^{10}Be ages of Seong et al. (2007) for the Skardu glacial stage being 157 ± 13 ka (M_w). Synchronous deposits for the Deshkit 1 and 2 glacial stages are not present in the central Karakoram.

The mean and standard error of the AAR, THAR, and AA methods give a contemporary ELA of 5510 ± 60 m a.s.l. for the contemporary Siachen Glacier. The ELA of the Deshkit 1 glacial stage (at ~45 ka) in the Nubra and Shyok valleys based on the AARB method of Osmaston (2005) is 5210 m a.s.l., which results in a ΔELA of 290 m.

The large difference in glacial extent between Karakoram and Ladakh Range is highlighted by the time equivalent Deshkit 1 to Deshkit 3 glacial stages (with Siachen Glacier extending >100 km) in the Nubra valley and morphostratigraphic equivalent moraines extending 2.7 ± 0.6 km (Deshkit 1), 9.2 ± 1.6 km (Deshkit 2), and ~33 km (Deshkit 3) from the present glaciers in the Ladakh Range tributary valleys. This illustrates the strong contrasts in patterns of glaciation across adjacent mountain ranges in the Himalayan–Tibetan orogen and emphasizes the need for caution when correlating regional glacial successions through high mountains.

Acknowledgments

JD thanks the Department of Geology, University of Cincinnati for supporting this study as part of his doctoral research, and Sigma Xi, the American Alpine Club, and the University Research Counsel of the University of Cincinnati for helping to fund this study; Byron Adams for helping to process samples during the early stages of this project, and Susan Ma for helping calculate our ^{10}Be ages and recalculate ages from other studies. LAO and MWC thank the Department of Geology at UC for helping to fund fieldwork. Thanks to Professor Alan Gillespie, Dr. Balco and an anonymous reviewer for comments on an earlier version of this paper.

References

Balco, G., Stone, J.O., Lifton, N.A., Dunai, T.J., 2008a. A complete and easily accessible means of calculating surface exposure ages or erosion rates from 10Be and 26Al measurements. Quaternary Geochronology 8, 174–195.

Balco, G., Briner, J., Finkel, R.C., Rayburn, J., Ridge, J.C., Schaefer, J.M., 2008b. Regional beryllium-10 production rate calibration for late-glacial northeastern North America. Quaternary Science Reviews 4, 93–107.

Benn, D.I., Lehmkuhl, F., 2000. Mass balance and equilibrium-line altitudes of glaciers in high mountain environments. Quaternary International 65 (66), 15–29.

Benn, D.I., Owen, L.A., 2002. Himalayan glacial sedimentary environments: a framework for reconstructing and dating former glacial extents in high mountain regions. Quaternary International 97 (98), 3–26.

Benn, D.I., Owen, L.A., Osmaston, H.A., Seltzer, G.O., Porter, S.C., Mark, B., 2005. Reconstruction of equilibrium-line altitudes for tropical and sub-tropical glaciers. Quaternary International 138 (139), 8–21.

Bhutiyani, M.R., 2000. Sediment load characteristics of a proglacial stream of Siachen Glacier and the erosion rate in Nubra valley in the Karakoram Himalayas, India. Journal of Hydrology 227, 84–92.

Bookhagen, B., Thiede, R.C., Strecker, M.R., 2005. Late Quaternary intensified monsoon phases control landscape evolution in the northwest Himalaya. Geology 33, 149–152.

Bookhagen, B., Burbank, D.W., 2006. Topography, relief, and TRMM-derived rainfall variations along the Himalaya. Geophysical Research Letters 33, L08405.

Briner, J.P., Kaufman, D.S., Manley, W.F., Finkel, R.C., Caffee, M.W., 2005. Cosmogenic exposure dating of late Pleistocene moraine stabilization in Alaska. Geologic Society of America Bulletin 117, 1108–1120.

Brown, E.T., Bendick, R., Bourlés, D.L., Gaur, V., Molnar, P., Raisbeck, G.M., Yiou, F., 2003. Early Holocene climate recorded in geomorphological features in western Tibet. Palaeogeography, Palaeoclimatology, Palaeoecology 199, 141–151.

CGIAR-CSI, 2007, 2007. The CGIAR Consortium for Spatial Information. http://srtm.csi.cgiar.org/SELECTION/inputCoord.asp.

Chevalier, M.L., Ryerson, F.J., Tapponnier, P., Finkel, R.C., Van Der Woerd, J., Haibing, L., Qing, L., 2005. Slip-rate measurements on the Karakoram Fault may imply secular variations in fault motion. Science 307, 411–414.

Derbyshire, E., 1981. Glacier regime and glacial sediment facies: a hypothetical framework for the Qinghai-Xizang Plateau. Proceedings of the Symposium on Qinghai-Xizang (Tibet) Plateau Beijing China: Vol. 2—Geological and Ecological Studies of Qinghai-Xizang Plateau. Science Press, Beijing, pp. 1649–1656.

Desilets, D., Zreda, M., 2003. Spatial and temporal distribution of secondary cosmic-ray nucleon intensities and applications to in-situ cosmogenic dating. Earth and Planetary Science Letters 206 (1–2), 21–42.

Dortch, J., Owen, L.A., Haneberg, W.C., Caffee, M.W., Dietsch, C., Kamp, D.U., 2008. Nature and timing of large-landslides in the Himalaya and Transhimalaya of northern India. Quaternary Science Reviews 28, 1037–1054.

Dortch, J.M., Owen, L.A., Caffee, M.W., 2009. Late Quaternary glaciation and ELA variations of the McKinley River region, central Alaska Range. Boreas 39, 223–246. doi:10.1111/j.1502-3885.2009.00121.

Dunlap, W.J., Weinberg, R.F., Searle, M.P., 1998. Karakoram fault zone rocks cool in two phases. Geological Society of London 155, 903–912.

Gasse, F., Fontes, J.C., Van Campo, E., Wei, K., 1996. Holocene environmental changes in Bangong Co basin (Western Tibet). Part 4: discussion and conclusions. Paleogeography, Paleoclimatology, Paleoecology 120, 79–92.

Hewitt, K., 1989. The altitudinal organization of Karakoram geomorphic processes and depositional environments. Zeitschrift für Geomorphologie 76, 9–32.

Kohl, C.P., Nishiizumi, K., 1992. Chemical isolation of quartz for measurements of in-situ-produced cosmogenic nuclides. Geochimica et Cosmochimica Acta 56, 3583–3587.

Kulkarni, A.V., 1992. Mass balance of Himalayan glaciers using AAR and ELA methods. Journal of Glaciology 38, 101–104.

Ma, X.Z., Li, Y.K., Bourgeois, M., Caffee, M.W., Elmore, D., Granger, D., Muzikar, P., Smith, P., 2007. Webcn: a web-based computation tool for in situ-produced cosmogenic nuclides. Nuclear Instruments & Methods in Physics Research Section B-Beam Interactions with Materials and Atoms 259, 646–652.

McDougall, I., Harrison, T.M., 1999. Geochronology and Thermochronology by the 40Ar/39Ar method, Second edition. Oxford University Press, Oxford. 269 pp.

Müller, F., 1980. Present and late Pleistocene equilibrium line altitudes in the Mount Everest region: an application of the glacier inventory. World Glacier Inventory 126, 75–94.

NASA, 2007. National Aeronautics and Space Administration Land Processes Distributed Active Archive Center, Earth Observing Data Gateway. http://edcimswww.cr.usgs.gov/pub/imswelcome/.

Nash, 2007. ReadArcGrid: histograms elevations read from datasets in ASCII AcGrid format. Also calculates dimensionless hypsometric curve. http://homepages.uc.edu/~nashdb/.

Nishiizumi, K., Wintterer, E.L., Kohl, C.P., Klein, J., Middleton, R., Lal, D., Arnold, J.R., 1989. Cosmic ray production of ^{10}Be and ^{26}Al in quartz from glacially polished rocks. Journal of Geophysical Research 94, 17907–17915.

Nishiizumi, K., Imamura, M., Caffee, M.W., Southon, J.R., Finkel, R.C., McAninch, J., 2007. Absolute calibration of ^{10}Be AMS standards. Nuclear Instruments & Methods in Physics Research—Beam Interactions with Materials and Atoms 258B, 403–413.

Osmaston, H., 2005. Estimates of glacier equilibrium line altitudes by the area × altitude, the area × altitude balance ration and the area × altitude balance index methods and their validation. Quaternary International 138–139, 22–31.

Owen, L.A., Gualtieri, L., Finkel, R.C., Caffee, M.W., Benn, D.I., Sharma, M.C., 2001. Cosmogenic radionuclide dating of glacial landforms in the Lahul Himalaya, Northern India: defining the timing of Late Quaternary glaciation. Journal of Quaternary Science 16, 555–563.

Owen, L.A., Ma, H., Derbyshire, E., Spencer, J.Q., Barnard, P.L., Nian, Z.Y, Finkel, R.C., Caffee, M.W., 2003. The timing and style of Late Quaternary glaciation in the La Ji mountains NE Tibet: evidence for restricted glaciation during the latter part of the Last Glacial. Zeitschrift für Geomorphology 130, 263–276.

Owen, L.A., Benn, D.I., 2005. Equilibrium-line altitudes for the Last Galial Maximum for the Himalaya and Tibet: an assessment and evaluation of results. Quaternary International 138 (139), 55–78.

Owen, L.A., Caffee, M.W., Bovard, K.R., Finkel, R.C., Sharma, M.C., 2006. Terrestrial cosmogenic nuclide surface exposure dating of the oldest glacial successions in the Himalayan orogen: Ladakh Range, northern India. Geological Society of America, Bulletin 118, 383–392.

Owen, L.A., Caffee, M.W., Finkel, R.C., Seong, B.Y., 2008. Quaternary glaciations of the Himalayan–Tibetan orogen. Journal of Quaternary Science 23, 513–531.

Owen, L.A., Robinson, R., Benn, D.I., Finkel, R.C., Davis, N.K., Yi, C., Putkonen, J., Li, D., Murray, A.S., 2009. Quaternary glaciation of Mount Everest. Quaternary Science Reviews 28, 1412–1433.

Pant, R.K., Phadtare, N.R., Chamyal, L.S., Juyal, N., 2005. Quaternary deposits in Ladakh and Karakoram Himalaya: a treasure trove of the paleoclimate records. Current Science 88, 1789–1798.

Phartiyal, B., Sharma, A., Upadhyay, R., Ram-Awatar, Sinha, A.K., 2005. Quaternary geology, tectonics and distribution of palaeo- and present flivio/glacio lacustrine deposits in Ladakh, NW Indian Himalaya—a study based on field observations. Geomorphology 65, 241–256.

Phillips, W.M., Sloan, V.F., Shroder Jr., J.F., Sharma, P., Clarke, M.L., Rendell, H.M., 2000. Asynchronous glaciation at Nanga Parbat, northwestern Himalaya Mountains, Pakistan. Geology 28, 431–434.

Prell, W.L., Kutzbach, J.E., 1987. Monsoon variability over the past 150, 000 years. Journal of Geophysical Research 92, 8411–8425.

PRIME Laboratory, 2007. PRIME laboratory rock age calculator. https://www.physics.purdue.edu/ams/rosetest/Rkversion1/rockpara.php.

PRIME Laboratory, 2010. Important note concerning ^{10}Be results. http://www.physics.purdue.edu/primelab/News/news0907.php.

Richards, B.W.M., Benn, D.I., Owen, L.A., Rhodes, E.J., Spencer, J.Q., 2000a. Timing of Late Quaternary glaciations south of Mount Everest in the Khumbu Himal, Nepal. Geological Society of American Bulletin 112, 1621–1632.

Richards, B.W.M., Owen, L.A., Rhodes, E.J., 2000b. Timing of Late Quaternary glaciations in the Himalayas of northern Pakistan. Journal of Quaternary Science 15, 283–297.

Searle, M.P., Dewey, J.F., Dunlap, W.J., Strachan, R.A., Weinberg, R.F., 1998. Transpressional tectonics along the Karakoram fault zone, northern Ladakh; constraints on Tibetan extrusion. Geological Society Special Publications; Continental Transpressional and Transtensional Tectonics 135, 307–326.

Searle, M.P., Richard, J.P., 2007. Relationships between right–lateral shear along the Karakoram fault and metamorphism, magmatism, exhumation and uplift: evidence from the K2-Gasherbrum, Pangong ranges, north Pakistan and Ladakh. Geological Society of London 164, 439–450.

Seong, Y.B., Owen, L.A., Bishop, M.P., Bush, A., Clendon, P., Copland, L., Finkel, R., Kamp, U., Shroder Jr., J.F., 2007. Quaternary glacial history of the Central Karakoram. Quaternary Science Reviews 26, 3384–3405.

Seong, Y.B., Bishop, M.P., Bush, A., Clendon, P., Copland, P., Finkel, R., Kamp, U., Owen, L.A., Shroder, J.F., 2008. Landforms and landscape evolution in the Skardu, Shigar and Braldu Valleys, Central Karakoram Mountains. Geomorphology 103, 251–267.

Seong, Y.B., Owen, L.A., Yi, C., Finkel, R.C., 2009. Quaternary glaciation of Muztag Ata and Kongur Shan: evidence for glacier response to rapid climate changes through the Late Glacial and Holocene in westernmost Tibet. Geological Society of America Bulletin 121, 348–365.

Shi, Y., Yu, G., Liu, X., Li, B., Yao, T., 2001. Reconstruction of the 30–40 ka BP enhanced Indian monsoon climate based on geological records from the Tibetan Plateau. Paleogeography, Paleoclimatology, Paleoecology 169, 69–83.

Stone, J.O., 2000. Air pressure and cosmogenic isotope production. Journal of Geophysical Research 105, 23753–23759.

Zech, W., Glaser, B., Ni, A., Petrov, M., Lemzin, I., 2000. Soil as indicators of the Pleistocene and Holocene landscape history: Alay Range (Khyrgstan). Quaternary International 65 (66), 161–170.

Zech, W., Glaser, B., Abramowski, U., Dittmar, C., Kubik, P.W., 2003. Reconstruction of the Late Quaternary Glaciation of the Macha Khola valley (Gorkha Himal, Nepal) using relative and absolute (^{14}C, ^{10}Be, dendrochronology) dating techniques. Quaternary Science Reviews 22, 2253–2265.

Zech, R., Abramowski, U., Glaser, B., Sosin, P., Kubik, P.W., Zech, W., 2005. Late Quaternary glacier and climate history of the Pamir Mountains derived from cosmogenic ^{10}Be exposure ages. Quaternary Research 64, 212–220.